Geomechanics and Engineering, *Vol. 18, No. 6 (2019) 627-638*
DOI: https://doi.org/10.12989/gae.2019.18.6.627

Effect of confining stress on representative elementary volume of jointed rock masses

Na Wu, Zhengzhao Liang*, Yingchun Li, Xikun Qian and Bin Gong

State Key Laboratory of Coastal and Offshore Engineering, Dalian University of Technology, Dalian, 116024, China

(Received June 17, 2019, Revised July 24, 2019, Accepted August 3, 2019)

Abstract. Estimation of representative elementary volume (REV) of jointed rock masses is critical to predict the mechanical behavior of field-scale rock masses. The REV of jointed rock masses at site is strongly influenced by stress state. The paper proposed a method to systematically studied the influence of confining stress on the REV of jointed rock masses with various strengths (weak, medium and strong), which were sourced from the water inlet slope of Xiaowan Hydropower Station, China. A finite element method considering material heterogeneity was employed, a series of two-dimensional (2D) models was established based on the Monte-Carlo method and a lot of biaxial compressive tests were conducted. Numerical results showed that the REV of jointed rock masses presented a step-like reduction as the normalized confining stress increased. Confining stress weakened the size effect of jointed rock masses, indicating that the REV determined under uniaxial compression test can be reasonably taken as the REV of jointed rock masses under complexed in-situ stress environment.

Keywords: numerical simulation; confining stress; scale effect; representative elementary volume; jointed rock masses

1. Introduction

Understanding the mechanical behaviors of jointed rock masses is crucial for predicting the stable of rock engineering projects (Li *et al.* 2019, Gao *et al.* 2019, Huang *et al.* 2019, Oh *et al.* 2019). The strength, deformation and failure characteristics of jointed rock masses are dependent heavily on the sample scale (named scale effect) until the sample size exceeds a critical value (Heuze 1980, Krauland *et al.* 1989). The magnitude of the critical value is termed the representative elementary volume (REV) (Hill 1963, Bear 1972, Long *et al.* 1982). The existence of REV enables us to treat rock masses as an equivalent continuum without considering the complicated joint system. Therefore, large-scale rock engineering structures can be conveniently simulated using the numerical simulation method, when major discontinuities (large size single feature) are only considered. Rock engineering projects, e.g., tunnels, rock slopes and deep underground openings, are commonly situated in higher in-situ stress environment. Therefore, the influence of confining stress on the REV of jointed rock masses is required for the design, operation and stability assessment of rock engineering projects.

Various methods have been used to determinate the REV. Analytical solutions (Amadei 1981) and empirical methods (e.g. GSI, Q, RMR) (Bieniawski 1978, Barton 2002) are two approaches widely used to estimate the REV of jointed rock masses. These methods are unable to estimate the REV of the jointed rock masses with sufficient accuracy since the variation of confining stress and loading conditions cannot be considered. Laboratory studies that experiment rock samples with limited number joints have been conducted to understand the mechanical properties of jointed rock masses (Heuze 1980, Darlington *et al.* 2011). However, few samples have been prepared with size that reached the REV due to the experimental difficulties. Additionally, the mechanical behaviors of field-scale jointed rock masses cannot be extrapolated through the behavior of an idealized rock sample at the laboratory scale (Ribacchi 2000, Khani *et al.* 2013). The REV of jointed rock masses can also be determined through in-situ testing (Neuman 1987, Cuisiat and Haimson 1992). But undertaking such tests is expensive and impracticable.

Numerical simulation has been proven to be an alternative method to simulate the REV of jointed rock masses, due to its advantage to calculate the complex joint geometry system. The REV is closely associated with the joint geometric parameters of the joint network, which we refer to geometrical REV. Oda and Masanobu (1988) recommended the relation between the geometrical REV and the typical length of joint traces. Kulatilake (1985) and Pariseau *et al.* (2008) successfully applied the finite element method (FEM) to investigate the scale effect of strength and deformation parameters of jointed rock masses, whereby the mechanical REV is determined. Khani *et al.* (2013) used the distinct element method to investigate the effect of the fracture intensity on the REV of the deformation modulus and Poisson's ratio of jointed rock masses. The geometrical and mechanical REVs of jointed rock mas were estimated using synthetic rock masses models by Esmaieli *et al.* (2010). Wang *et al.* (2002) applied the discrete fracture fluid flow model to determine the REV size for the rock masses with respect to hydraulic behavior.

Existing studies mainly focus on the REV of jointed rock masses subjected to uniaxial compression. The

*Corresponding author, Professor
E-mail: LiangZZ@dlut.edu.cn

ISSN: 2005-307X (Print), 2092-6219 (Online)

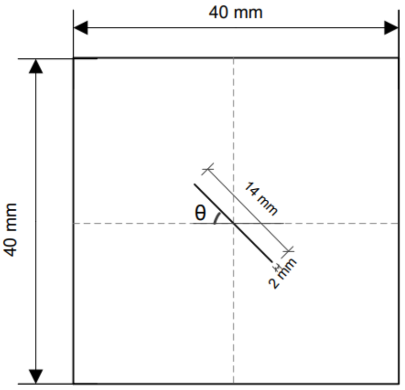

(a) The model containing a single joint

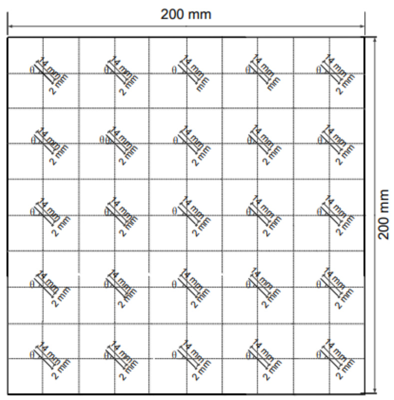

(b) The model containing twenty-five joints

Fig. 1 The layout of the partial tested models

mechanical behaviors of jointed rock masses are affected appreciably by the confining stress (Prudencio and Jan 2007, Cai 2008, Yang *et al.* 2015b, Lei *et al.* 2017). Tremendous efforts have been made to study the influence of the confining stress on the equivalent strength and deformability properties of jointed rock masses based on the REV determined on uniaxial compression (Baghbanan 2008, Bidgoli and Jing 2014, Yang *et al.* 2015a, Laghaei *et al.* 2018, Vazaios *et al.* 2018). However, the influence of the confining stress on the REV of jointed rock masses is often ignored.

The paper numerically studies the influence of confining stress on the scale effect of jointed rock masses of different strengths (weak, medium and strong). The jointed rock masses of the water inlet slope of Xiaowan Hydropower Station, China is taken as an example, and a FEM code considering the material heterogeneity and the joint probability distribution is used to study the issue. Firstly, the validity of the FEM code is verified by comparing with the experimental results. Furthermore, three different two-dimensional discrete fracture network models are established based on the Monte-Carlo method and the joint probability distribution. Then, a series of biaxial compression tests is conducted to investigate the effect of the confining stress on the strength and deformation characteristics as well as the REV of jointed rock masses. Finally, the effects of joint system (joint dip angle and joint intensity) on the stress-dependency of the REV are reported.

2. Numerical simulation

2.1 Validation of the RFPA^{2D}

Two-dimensional rock failure process analysis (RFPA^{2D}), which was proposed in 1995 by Tang (1997), is employed as the basic rock failure analysis tool. The heterogeneity of rocks and joints at a mesoscopic level can be considered by assuming that the rock and joint properties (i.e., elastic modulus) obey the Weibull distribution. Elastic damage mechanics is used for describing the constitutive law of single meso-level element. The maximum tensile strain criterion and Mohr-Coulomb failure criterion are employed as the damage threshold. The finite element in the RFPA^{2D} will be considered to fail in the tensile pattern when its minimum principal stress exceeds the tensile strength, and to fail in the compressional shear pattern when the compression-shear stress satisfies the Mohr-Coulomb criterion. Additional details on the RFPA simulation have been extensively presented (Wong *et al.* 2002, Li and Tang *et al.* 2015).

Fig. 2 Experimental samples with 60º joint inclination angle

To verify the effectiveness of RFPA^{2D} to study the scale effect of jointed rock masses, the idealized jointed rock specimens with various sizes are simulated using RFPA^{2D} and the results are compared with the related laboratory results. The sizes of the tested models in the dimensions of high, width and thickness are 40 mm × 40 mm × 80 mm, 80 mm × 80 mm × 80 mm, 120 mm × 120 mm × 80 mm, 160 mm × 160 mm × 80 mm, 200 mm × 200 mm × 80 mm, respectively. Correspondingly, the number of the penetrated joints in the tested models are 1, 4, 9, 16 and 25, respectively. Fig. 1(a) shows the layout of the tested model containing a single joint. The other layouts of the tested models are the accumulation of the single joint models. For example, the layout of the tested model containing twenty-five joints are shown in Fig. 1(b). In the tested models, the joint is penetrated through the model thickness, and the length and width of joint are fixed at 12 mm × 2 mm. Furthermore, the inclination angles θ (the angle of the joint with the direction of the horizontal direction) of the transfixion joints in the tested model are fixed at 60º and 75º, respectively.

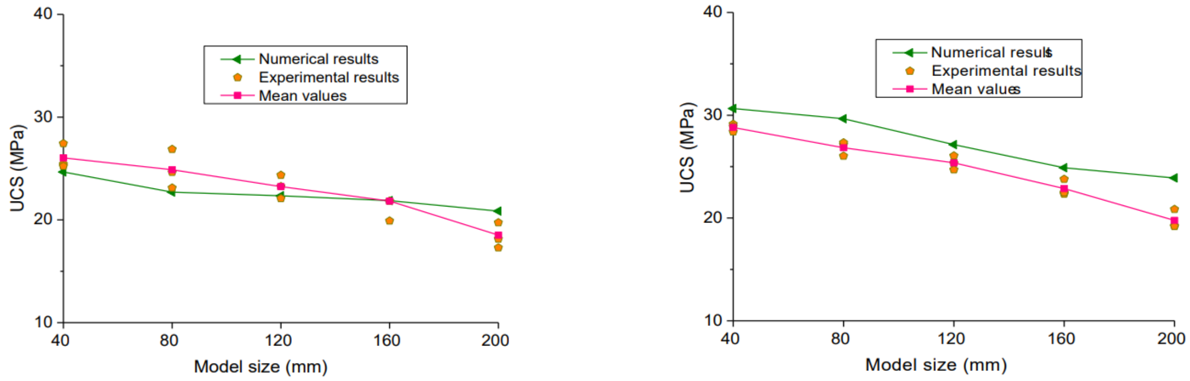

(a) Models with 60° joint inclination angle (b) Models with 75° joint inclination angle

Fig. 3 Comparison of UCS between the experimental and numerical results

(a) Four joints model with 60° inclination angle (b) Nine model with 75° joint inclination angle

Fig. 4 Comparison of failure patterns between the experimental and numerical results

Table 1 Probability statistical distribution of joint parameters (Wang *et al.* 2010)

Joint parameters in weak-strength rock masses		#1	#2	#3
Dip angle (°)	Type	I	I	I
	Mean value	74.78	87.48	39.27
	Standard deviation	8.69	13.29	8.33
Trace length (m)	Type	II	I	II
	Mean value	2.44	1.97	1.72
	Standard deviation	0.34	0.36	1.35
Spacing (m)	Type	II	I	II
	Mean value	0.33	0.26	0.44
	Standard deviation	0.33	0.26	0.78
Joint parameters in mediate-strength rock masses		#1	#2	#3
Dip angle (°)	Type	I	I	I
	Mean value	80.26	89.3	42.88
	Standard deviation	9.91	9.25	6.54
Trace length (m)	Type	II	II	II
	Mean value	2.54	1.56	1.52
	Standard deviation	1.39	1.01	0.87
Spacing (m)	Type	III	II	III
	Mean value	0.3	0.31	0.29
	Standard deviation	0.3	0.44	0.29
Joint parameters in strong-strength rock masses		#1	#2	#3

Table 1 Continued

Joint parameters in weak-strength rock masses		#1	#2	#3
Dip angle (°)	Type	I	I	IV
	Mean value	81.86	86.83	40.44
	Standard deviation	10.06	11.59	7.41
Trace length (m)	Type	II	II	II
	Mean value	2.14	1.36	0.76
	Standard deviation	1.45	0.98	0.55
Spacing (m)	Type	III	III	III
	Mean value	0.40	0.34	0.54
	Standard deviation	0.40	0.34	0.54

The experimental samples with joint inclination angle of 60° is illustrated in Fig. 2. For each tested experimental sample, three cement mortar specimens, which is a mixture of C42.5 cement, fine sand and water with the weight ratio of 2:2:1, are prepared to simulate the natural rock masses. The experimental samples are cured for 28 days (temperature is 20 ± 3°C and relative humidity is more than 95%) before being subjected to uniaxial compression test. The average values of unit weight, elastic modulus, UCS, tensile strength, frictional coefficient, cohesion and Poisson's ratio of the cement mortar material are evaluated as 2072.4 kg/m^3, 2.173 GPa, 34.522 MPa, 1.315 MPa, 37°, 2.748 MPa and 0.225, respectively, in laboratory test. A series of uniaxial compression tests is conducted using the RMT-150C Rock Mechanics Testing System. A constant axial displacement-controlled load of 0.002 mm/s is applied on the top of the experimental samples until failure occurs. Additionally, the corresponding numerical models are generated by using RFPA^{2D} and the displacement-controlled load of strain rate of 2.0e-5 per step is applied on the top of the models until failure occurs. The mechanical parameter values used in the RFPA^{2D} are obtained based on the laboratory test.

Fig. 3 shows the comparison of UCS between the experimental and numerical results. Results show that the values of the UCS gradually decrease with an increasing tested model size and show scale effect. It is worth noting that the numerical results for 60º are slightly lower than the related experimental results (Fig. 3(a)), while the numerical results for 75º are higher than the related experimental results (Fig. 3(b)). Comparison of failure patterns between the experimental and numerical results are given in Fig. 4. The models mainly show shear failure at the tips of the joints until the cracks connect and failure occurs. Overall, the scale effect and failure patterns of tested model in the numerical simulation coincide with the experimental tests.

Due to the limited test conditions, most laboratory sample studies on the size effect of jointed rock masses are in uniaxial compression. Therefore, it is a pity that the reliability of RFPA^{2D} to study the scale effect of jointed rock masses can only be verified under uniaxial compression. This is also the reason why the numerical method was used to study the effect of confining pressure on scale effect of jointed rock masses, especially for field scales. In addition, the RFPA^{2D} has been widely applied in investigating the strength and deformation behavior of jointed rock specimens at lab-scales (Xu *et al.* 2013, Li and Tang 2015), and the scale effect of jointed rock masses at field scales (Wang *et al.* 2016, Wu *et al.* 2019).

2.2 Engineering background

To investigate the impact of various rock types on the scale effect of jointed rock masses, the rocks of different strengths of the water inlet slope of Xiaowan Hydropower Station, China are studied. The main rock types of the slope are hornblende-plagioclase gneiss and biotite granite gneiss. Since there are no large faults, stability of the slope is mainly governed by small joints developing in the rock masses. According to different weathering degree, the rock masses of the water inlet slope are divided into three zones from the surface to the inside as weak-, medium- and strong-strengths rock masses. The geometric parameters of the joints in these three zones conform to the probability distribution. Field measurement is carried out by surveying lines, and a probability statistical model reflecting the distribution characteristics of the jointed rock masses is established. There are three sets of joints in each zone and the joint geometric parameters, e.g., trace length, dip angle and spacing are given in Table 1. Types I, II, III and IV in Table 1 stand for the normal distribution, the ogarithmic normal distribution, the negative exponential distribution and the uniform distribution, respectively.

2.3 Numerical model set-up

In the numerical model, accurate description of the probability statistical distribution of joints is the key to study the REV size and mechanical properties of jointed rock masses (Bandpey *et al.* 2018). According to the probability statistical distribution of joint geometric parameters of three different strength jointed rock masses (as shown in Table 1), the central coordinate of each trace line (x_c, y_c) supposed to uniform distribution were generated based on the Monte-Carlo method. Additionally, the specific values of the joint dip angle α and trace length l can be also obtained according to the probability distribution of the joint dip angle and trace length. According to the obtained x_c, y_c, α and l, the joints in the research area were drawn and their endpoint coordinates were stored in the computer. Then, three different discrete fracture network models of 20 m × 20 m are generated based on the Monte-Carlo method. The main advantage of this method is a detailed definition of the joint geometry and a realistic representation of the natural joint system. Then, the network datum are obtained and a series of square FEM models with various side lengths is constructed to investigate the mechanical properties of jointed rock masses by embedding the data into the RFPA^{2D}. The side lengths of the FEM models for weak jointed rock masses are 2 m, 4 m, 6 m, 8 m, 10 m, 12 m, and for mediate and strong jointed rock masses are 2 m, 4 m, 6 m, 8 m, 10 m, 12 m, 14 m, 16 m and 18 m, respectively. Fig. 5(a) shows the FEM models of mediate jointed rock masses using in the numerical simulation. The blue lines in Fig. 5(a) represent generated joints, and the concentric squares formed by pink lines represent the research regions for FEM models.

Table 2 The mechanical parameters of rocks and joint used in the numerical simulation

Material type	Heterogeneity index	Uniaxial compressive strength (MPa)	Elastic modulus (GPa)	Friction angle (°)	Poisson's ratio
Weak-strength rock	5	71.8	22.1	46	0.32
Mediate-strength rock	4	105.2	42.2	51	0.28
Strong-strength rock	3	145.8	46.2	55	0.18
Joint	2	4.44	1.84	28	0.34

In the numerical simulation, the plain strain model is adopted. The lower boundary of the numerical model is constrained in the vertical direction, and the confining stress σ_p is applied on the other surfaces of the model. After the model converges, an external displacement U at a constant rate of 0.00002 times the model side length in the axial direction is applied to the upper boundary of the numerical sample until sample fails (Yang and Jing 2011). The boundary condition and loading mode are shown in Fig. 5 (b). The confining stresses σ_p applied on the model are divided into ten grades and the value of confining stress σ_p generally does not exceed the uniaxial compressive strength of rock masses. In the work, the confining stresses σ_p are 0, 0.005, 0.01, 0.015, 0.02, 0.025, 0.03, 0.05, 0.1 and 0.15 times the uniaxial compressive strength of weak, mediate and strong rocks, respectively. For example, the uniaxial compressive strength of mediate rock is 105.2 MPa (as

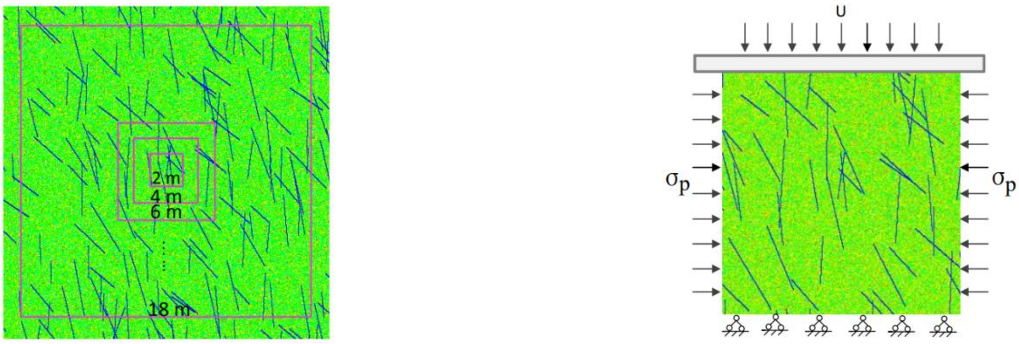

(a) Illustration of the study of scale effect (b) Typical set-up and boundary conditions

Fig. 5 Illustration and typical set-up and boundary conditions of model of medium-strength jointed rock masses

listed in Table 2), so the confining stresses σ_p applied on the FEM models are 0 MPa, 0.526 MPa, 1.052 MPa, 1.578 MPa, 2.104 MPa, 2.63 MPa, 3.156 MPa, 5.26 MPa, 10.52 MPa and 15.78 MPa, respectively. Then, a series of biaxial compression tests is conducted on the FEM models using RFPA^{2D}.

The rock masses of different strengths are considered to be composed of rock blocks and joints, both of which are assumed to be continuous medium with varying mechanical parameters. The mechanical parameters of the rock blocks are obtained by experimental tests on the rock samples collected from Xiaowan Hydropower Station, China. However, the mechanical parameters of joints were difficult to obtain based on the laboratory experiments. Generally, the mechanical parameters of joints are relatively lower than those of intact rocks and the values of which have generally been set to 1-20% that of intact rock (Pariseau *et al.* 2008, Zhou *et al.* 2018, Wu *et al.* 2019). In this paper, the parameters of rock blocks and joints used in the numerical calculation are listed in Table 2 and much lower mechanical parameters are assigned to the joints based on the previous suggestions.

3. Effect of confining stress and model size on the mechanical properties of jointed rock masses

3.1 Axial stress-strain curves of medium-strength jointed rock masses

The influence of confining stress and model size on the mechanical properties of jointed rock masses of different strengths are similar to each other. Therefore, the jointed rock masses in medium-strength are taken as an example to illustrate this issue. The effect of the confining stress increasing from 0 MPa to 2.630 MPa on the axial stress-strain curves of medium-strength jointed rock masses for the 10 m model is given in Fig. 6. Numerical results show that the confining stress has a limited effect on the deformation characteristics of the models before yielding stress is reached, whereas the slope of the straight line portion of the axial stress-strain curve increases with the increase of the confining stress. When the models reach yield states, the compressive strength increases with ascending confining stress, and the axial stress-strain curves follow a strain-hardening trend, which is consistent with previous studies (Bidgoli and Jing 2014, Yang *et al.* 2015a).

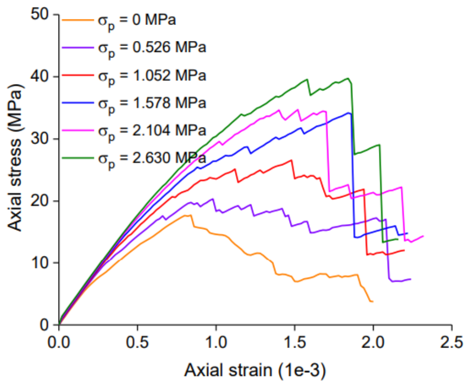

Fig. 6 Influence of confining stress (σ_p) on the axial stress-strain curves of medium-strength jointed rock masses for the 10 m model

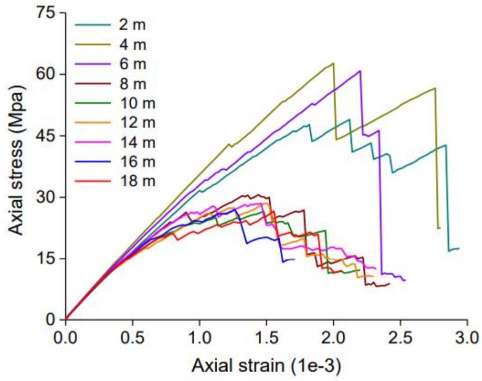

Fig. 7 Influence of model size under the 1.052 MPa confining stress on the axial stress-strain curves of the medium-strength jointed rock masses

The effect of model size increasing from 2 m to 18 m under the confining stress of 1.052 MPa on the axial stress-strain curves is shown in Fig. 7. According to Fig. 7, as model size increases, the axial stress-strain curve, compressive strength, slope of straight line portion of the axial stress-strain curves all manifest a distinct size effect with increasing model sizes.

3.2 Failure patterns of medium-strength jointed rock masses

Fig. 8 shows the failure patterns of medium-strength jointed rock masses as confining stress increases from 0

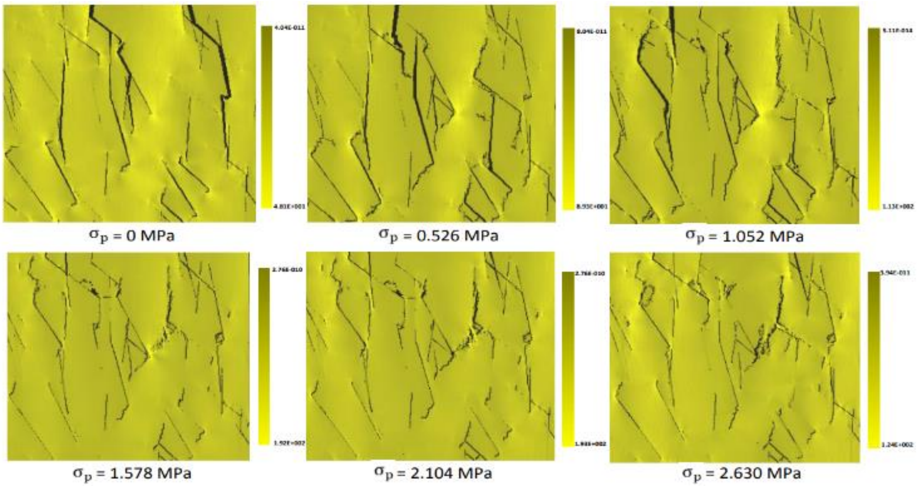

Fig. 8 Influence of confining stress (σ_p) on the failure patterns of medium-strength jointed rock masses for the 10 m model

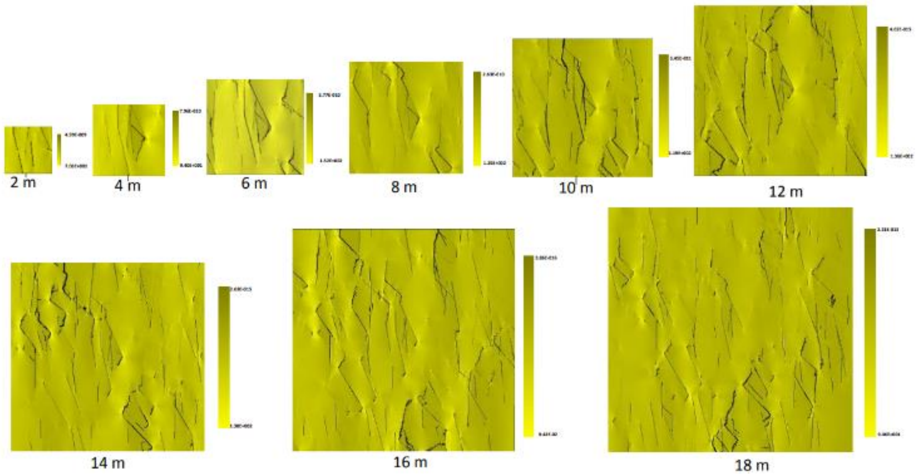

Fig. 9 Influence of model size under 1.052 MPa confining stress on the failure patterns of medium-strength jointed rock masses

MPa to 2.630 MPa for the 10 m model. Results show that tensile-shear composite failure mainly occurs along the joint planes and tensile failure often appears at the joint tips under various confining stresses. Therefore, the models show tensile-shear composite failure. Specifically, as the confining stress increases from 0 MPa to 1.052 MPa, the development of tensile-shear composite cracks along the joint planes is restrained while the growth of tensile crack at the tips of joints is fully promoted. When the confining stress further increases from 1.578 MPa to 2.630 MPa, both the tensile-shear composite failure along the joint planes and tensile failure at the tips of joints are restrained. Besides, new tensile failure occurs at rock bridges of the partial joints. Therefore, it is concluded that the confining stress has a limited influence on the failure patterns of the 10 m model, but increasing confining stress weakens the frictional sliding among joints, restrains lateral dilation of the models, and promotes the development of new shear joints at rock bridges.

The influences of model size increasing from 2 m to 18 m under 1.052 MPa confining stress on the failure patterns of medium-strength jointed rock masses are plotted in Fig. 9. As shown in Fig. 9, when the model side length is 2 m, the joints contained in the model are almost connected. The model is mainly controlled by one of the connected joints and undergoes tensile failure along the joint planes, which approximately parallel to the vertical direction (the dip angles of the joints in the model are mainly 80° and 89°, as shown in Table 1). When the model side length is larger than 2 m, the model contains several discontinuous joints. The shear failure firstly occurs along the joint planes and then tensile stress concentration appears in the tips of joints. The models mainly show tensile-shear composite failure. Therefore, the failure patterns of jointed rock masses are significant related to the model size, which contains complex joint geometric structures.

4. Effect of confining stress on REV of jointed rock masses

Fig. 10 shows the influence of confining stress on the compressive strength of jointed rock masses of different strengths. It can be seen that the compressive strength of the models first decreases and then remains unchanged for weak- and strong-strength jointed rock masses as model

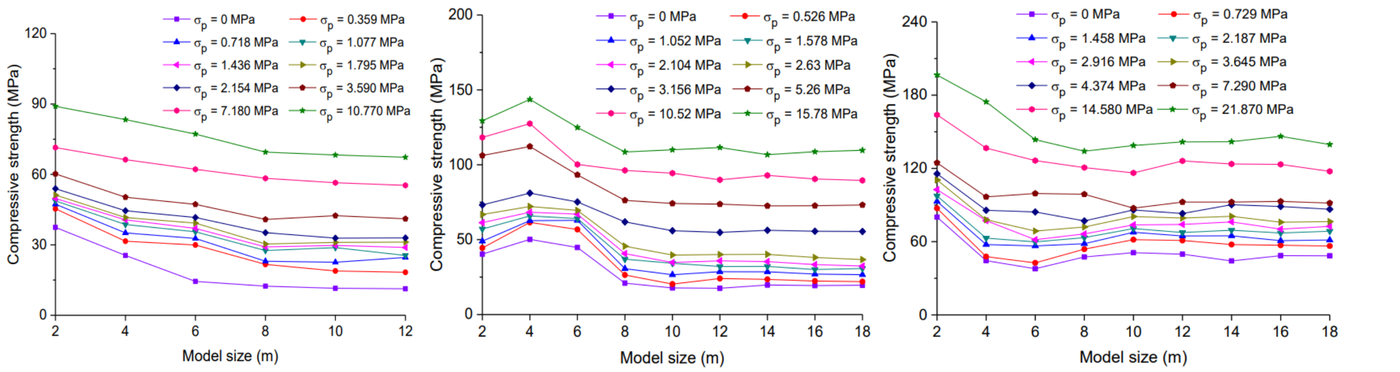

(a) Weak-strength (b) Medium-strength (c) Strong-strength

Fig. 10 Influence of confining stress (σ_p) on the compressive strength of jointed rock masses of different strengths

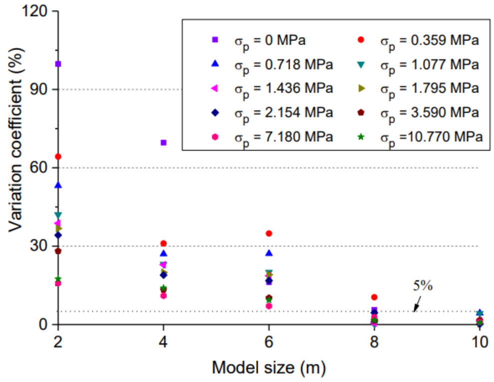

(a) Weak-strength

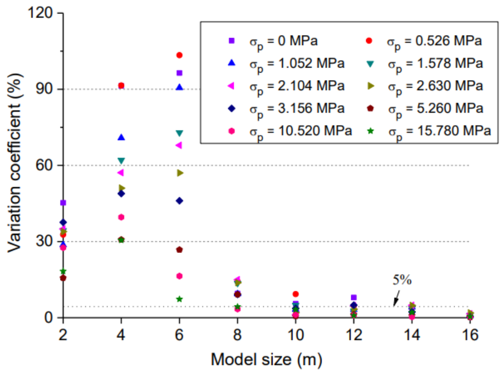

(b) Medium-strength

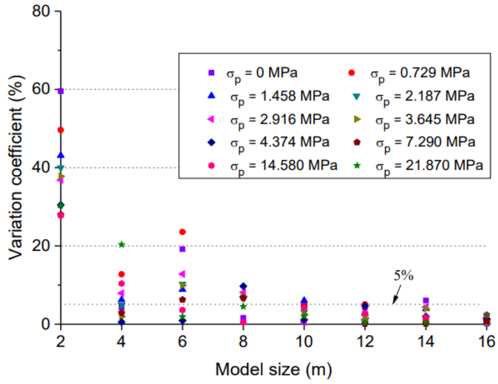

(c) Strong-strength

Fig. 11 Relationship between variation coefficient of compressive strength and model size of jointed rock masses of different strengths under various confining stresses

size increases under various confining stresses (Figs. 10(a) and (c)). It is noteworthy that when the model size increases from 2 m to 4 m, the compressive strength of medium-strength jointed rock masses increases with the increase of model size, as shown in Fig. 10(b). The main reason can be analyzed from the influence of joint geometric distribution on the mechanical properties of rock masses. When the model size is 2 m, there is a persistent joint in the model (as shown in Fig. 9), hence the compressive strength of the model with a size of 2 m is smaller than that of 4 m. In addition, the compressive strength of jointed rock masses in different strengths exhibits distinct size effect.

In general, the minimum volume beyond which the compressive strength tends to be stable as the model size increases is called the REV. In order to quantitatively analyze the effect of confining stress on the REV of compressive strength of jointed rock masses, the variation coefficients is given in Eq. (1)(Yang *et al.* 2015a)

$$K_i = \frac{|A_i - \bar{A}_i|}{\bar{A}_i} \tag{1}$$

where K_i is the variation coefficient of compressive strength, A_i is the compressive strength assessed by the RFPA^{2D} with model size of i, and $\bar{A}_i$ is the average compressive strength with a model size greater than or equal to i. In addition, the smaller the value of K_i produces smaller fluctuation in the compressive strength when the model size is greater than or equal to i.

Fig. 11 illustrates the relationship between the variation

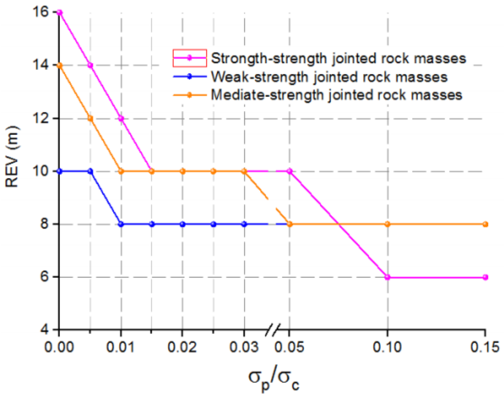

Fig. 12 Influence of normalized confining stress σ_p/σ_c on the REV of jointed rock masses of different strengths

coefficient of compressive strength and the model size of the jointed rock masses of different strengths under various confining stresses. Numerical results show that the K_i first fluctuates and then tends to be stable, which exhibits an obvious size effect with the increase of the model size. In this work, the acceptable error of the K_i is set to 5%. Correspondingly, the minimum model size beyond which the K_i is less than or equal to 5% is determined as the REV.

To quantify the relation of the REV and confining stress, the ratio of confining stress (σ_p) applied on the jointed rock masses to the UCS (σ_c) of intact rocks is defined as the normalized confining stresses (σ_p/σ_c). Therefore, the normalized confining stresses σ_p/σ_c of jointed rock masses of different strengths are 0, 0.005, 0.01, 0.015, 0.02, 0.025, 0.03, 0.05, 0.1 and 0.15.

Fig. 12 introduces the influence of σ_p/σ_c on the REV size of jointed rock masses in different strengths. For weak-strength jointed rock masses, the REV size keeps at 10 m × 10 m as the σ_p/σ_c increases from 0 to 0.005, then decreases to 8 m × 8 m as σ_p/σ_c increases to 0.01, and finally keeps a constant value of 8 m × 8 m as σ_p/σ_c increases to 0.15. For medium-strength jointed rock masses, the REV reduces from14 m × 14 m to 10 m × 10 m as σ_p/σ_c increases from 0 to 0.01, then remains constant at 10 m × 10 m as σ_p/σ_c increases to 0.03, and eventually declines again to a constant value of 8 m × 8 m as σ_p/σ_c increases to 0.15. For strong-strength jointed rock masses, the REV drops from 16 m × 16 m to 10 m × 10 m as σ_p/σ_c grows from 0 to 0.015, then remains constant at 10 m × 10 m as σ_p/σ_c increases to 0.05, and finally decreases again a constant value of 6 m × 6 m as σ_p/σ_c increases to 0.15. The results indicate that the REV of jointed rock masses present a step-like reduction as σ_p/σ_c increases. Therefore, the confining stress weakens the scale effect of the jointed rock masses and reduces the sensitivity of model size to the rock masses strength. At present, it is still a problem to accurately describe the magnitude and direction of the stress field of rock masses in complex rock engineering. The reason is that the stress state of rock masses is not only related to gravity, but also affected by the geological structure with various types and scales. Generally, it is obviously reasonable to regard the maximum REV as the REV of the study zone. Hence, the REV obtained under the uniaxial compression test can be used as the REV of jointed rock masses that subjected to complex stress conditions. This is of great significance in practical rock engineering application.

5. Discussions

The REV of jointed rock masses is significant influenced by the complex joint system (such as the joint dip angle and the joint density) (Khani *et al.* 2013, Zhang *et al.* 2013). To further understand of the effect of confining stress on the REV of jointed rock masses, three typical joint models containing various joint dip angles and joint densities (termed Models A, B and C) are established. The joint trace length is fixed at 0.8 m and follows a logarithmic normal distribution in the model. The joint dip angle and the joint spacing follow the logarithmic normal distribution and the negative exponential distribution, respectively. Furthermore, Model A contains a set of horizontal joints having a density of 3.5 m^{-2} (Fig. 13(a)). Given the same joint density, the joint dip angle in Model B is vertically rotated by 90° in the clockwise direction as shown in Fig. 13(b). Model C contains a set of horizontal joints, and the joint density is 0.2 times of that in the Model A, as shown in Fig. 13(c). The sizes of the square models of the three typical jointed rock masses are 2 m, 4 m, 6 m, 8 m, 10 m, 12 m and 14 m (Fig. 13). The mechanical parameters of rocks used in RFPA^{2D} are shown in Table 3. Much lower mechanical parameters are assigned to the joints. Finally, a series of biaxial compression tests is carried out, and the confining stresses applied on the models are 0 MPa, 5 MPa, 10 MPa, 15 MPa and 20 MPa, respectively. The loading method is the same as that in Section 2.

Under different confining stresses, the compressive strength of three typical joint models shows a significant scale effect (Fig. 14). The variation coefficients of compressive strength can be acquired according to Eq. (1), and the REVs of three typical joint models also can be got with an acceptable K_i of less than 5%. Fig. 15 shows the influence of confining stress on the REVs of three typical joint models. For Model A, the REV remains unchanged at 6 m × 6 m as the confining stress increases from 0 MPa to 20 MPa. The REV of Model B first keeps stable at 10 m × 10 m as the confining stress increases from 0 MPa to 5 MPa. With further increase of confining stress from 5 MPa to 10 MPa, the REV decreases to 8 m × 8 m and finally remains constant at this value. In addition, the REV of Model C first decreases from 10 m × 10 m to 8 m × 8 m as confining stress increases from 0 MPa to 5 MPa, and then keeps unchanged at 8 × 8 m. when the confining stress is greater than 5 MPa. It can be concluded that the influence of the confining stress on the REV of the jointed rock masses not only is affected by the joint dip angle, but also related to the magnitude of joint density.

To overcome computational limitations, the 3D joints were mapped into a 2D model. This is a widely used approach to investigate the scale effect and REV of jointed rock masses (Pouya and Ghoreychi 1998, Bidgoli and Jing 2014, Zhou *et al.* 2018). Previous studies have successfully

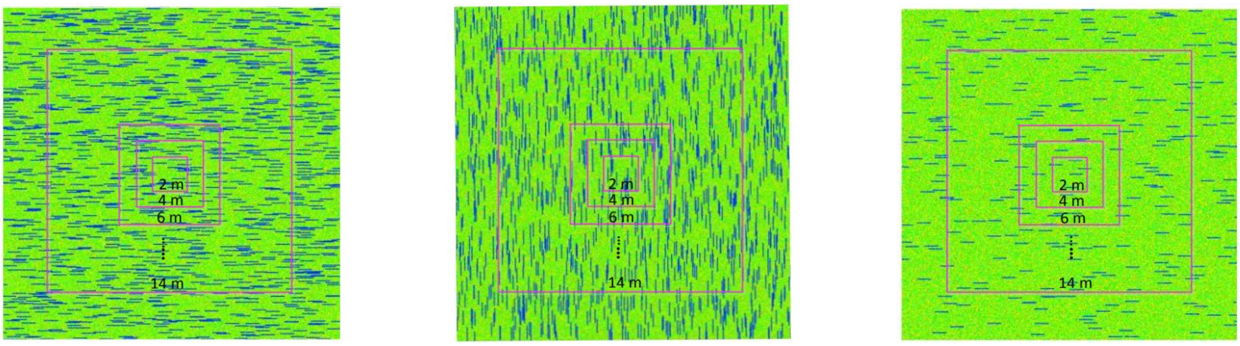

(a) Model A (b) Model B (c) Model C

Fig. 13 Model set-up for three typical joint models

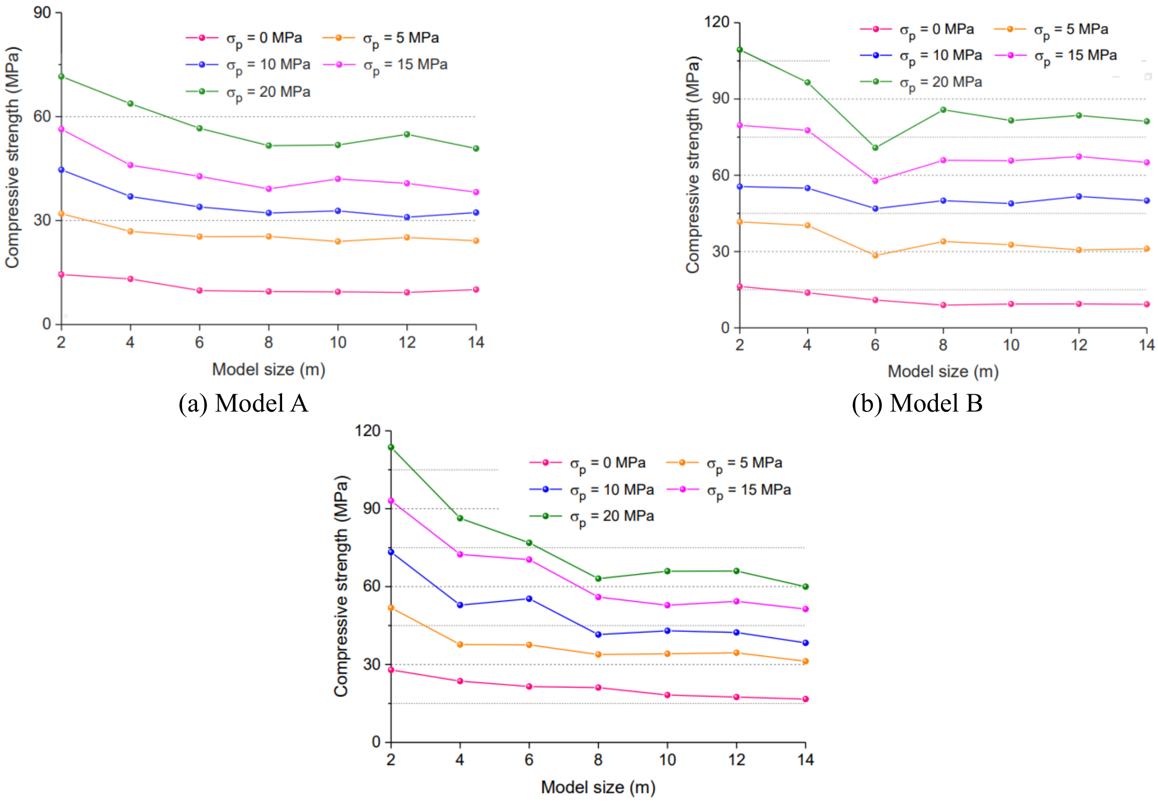

(a) Model A (b) Model B

(c) Model C

Fig. 14 Influence of confining stress (σ_p) on the compressive strength of three typical joint models

Table 3 The mechanical parameters of rock and joint used in the numerical simulation

Material type	Heterogeneity index	Uniaxial compressive strength (MPa)	Elastic modulus (GPa)	Friction angle (°)	Poisson's ratio
Rock	5	100	15	51	0.28
Joint	2	5	0.75	28	0.34

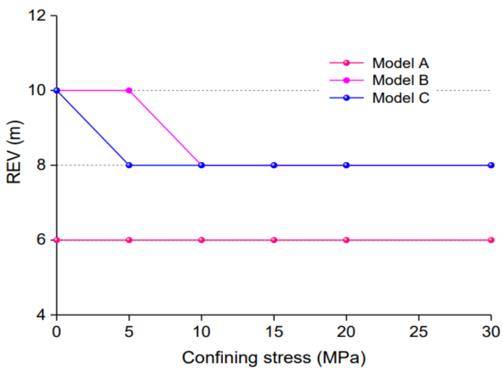

Fig. 15 Influence of confining stress on the REV of three typical joint models

demonstrated the viability of this simplification. Additionally, the equivalent mechanical parameters of jointed rock masses in in-situ stress environment can be obtained by considering the anisotropic behavior of the rock masses based on the REV size determined under the uniaxial compression test. It lays a foundation for the study of field-scale engineering problem using the equivalent continuum model. Finally, the paper provided a method to determine the REV size of jointed rock masses under various stress environment, and the results obtained are based on two-dimensional simulation model. More knowledge related to three-dimensional cases demands to be further studied.

5. Conclusions

• A series of two-dimensional (2D) joint network models was established based on the Monte-Carlo method and a lot of biaxial compressive tests were conducted to study the scale effect of the jointed rock masses of different strengths. The numerical results suggested that the compressive strength of jointed rock masses of different strengths exhibited distinct size effect under various confining stresses.

• The REVs of the jointed rock masses of different strengths were obtained with an acceptable variation coefficient of less than 5% under various normalized confining stress. Numerical results showed that the REVs of the jointed rock masses of different strengths presented a step-like reduction as normalized confining stress increased. This indicated the confining stress weakened the scale effect of the jointed rock masses and reduced the sensitivity of the model size to the rock masses strength.

• Jointed rock masses are commonly situated under complex in-situ stress environment. The REV of jointed rock masses is significantly affected by confining stress, and generally decreased as confining stress increases. The REV determined under uniaxial compression test is greater than that determined under biaxial compression test. Therefore, the REV determined under uniaxial compression test can be treated as the REV of jointed rock masses of rock-engineering structures in the field.

Acknowledgments

This study is supported by the National Natural Science Foundation of China (Grant No. 51779031 and 41977219).

References

Amadei, B. and Goodman, R. (1981), "A 3-D constitutive relation for fractured rock masses", *Proceedings of the International Symposium on the Mechanical Behavior of Structure Media*, Ottawa, Canada, October.

Bear, J. (1972), "Dynamics of fluids in porous media", *Eng. Geol.*, **7**(2), 174-175. https://doi.org/10.1016/0013-7952(73)90047-1.

Bieniawski, Z.T. (1978), "Determining rock mass deformability: Experience from case histories", *Int. J. Rock Mech. Min. Sci.*, **15**(5), 237-247. https://doi.org/10.1016/0148-9062(78)90956-7.

Barton, N. (2002), "Some new Q-value correlations to assist in site characterization and tunnel design", *Int. J. Rock Mech. Min. Sci.*, **39**(2), 185-216. https://doi.org/10.1016/S1365-1609(02)00011-4.

Baghbanan, A. (2008), "Scale and stress effects on hydro-mechanical properties of fractured rock masses", Ph.D. Dissertation, KTH Royal Institute of Technology, Stockholm, Sweden.

Bidgoli, M.N. and Jing, L. (2014), "Anisotropy of strength and deformability of fractured rocks", *J. Rock Mech. Geotech. Eng.*, **6**(2), 156-164. https://doi.org/10.1016/j.jrmge.2014.01.009.

Bandpey, A.K., Shahriar, K., Sharifzadeh, M. and Marefvand, P. (2018), "Validation of 3D discrete fracture network model focusing on areal sampling methods-a case study on the powerhouse cavern of Rudbar Lorestan pumped storage power plant, Iran", *Geomech. Eng.*, **16**(1), 21-34. https://doi.org/10.12989/gae.2018.16.1.021.

Cuisiat, F.D. and Haimson, B.C. (1992), "Scale effects in rock mass stress measurements", *Int. J. Rock Mech. Min. Sci.*, **29**(2), 99-117. https://doi.org/10.1016/0148-9062(92)92121-R.

Cai, M. (2008), "Influence of intermediate principal stress on rock fracturing and strength near excavation boundaries-insight from numerical modeling", *Int. J. Rock Mech. Min. Sci.*, **45**(5), 763-772. https://doi.org/ 10.1016/0148-9062(78)90956-7.

Darlington, W.J., Ranjith, P.G. and Choi S.K. (2011), "The effect of specimen size on strength and other properties in laboratory testing of rock and rock-like cementitious brittle materials", *Rock Mech. Rock. Eng.*, **44**(5), 513-529. https://doi.org/10.1007/s00603-011-0161-6.

Esmaieli, K., Hadjigeorgiou, J. and Grenon, M. (2010), "Estimating geometrical and mechanical REV based on synthetic rock mass models at Brunswick Mine", *Int. J. Rock Mech. Min. Sci.*, **47**(6), 915-926. https://doi.org/10.1016/j.ijrmms.2010.05.010.

Gao, M., Liang, Z.Z, Jia, S.P, Li, Y.C and Yang, X.X. (2019), "An equivalent anchoring method for anisotropic rock masses in underground tunnelling", *Tunn. Undergr. Sp. Technol.*, **85**, 294-306. https://doi.org/10.1016/j.tust.2018.12.017.

Hill R.j. (1963), "Elastic properties of reinforced solids: Some theoretical principles", *J. Mech. Phys. Solids*, **11**(5), 357-372. https://doi.org/ 10.1016/0022-5096(63)90036-X.

Heuze, F.E. (1980), "Scale effects in the determination of rock mass strength and deformability", *Rock Mech. Rock. Eng.*, **12**(3-4), 167-192. https://doi.org/10.1007/BF01251024.

Hoek, E. (1983), "Underground excavations in rock", *Eng. Geol.*, **19**(3), 244-246. https://doi.org/10.1016/0013-7952(83)90009-1.

Huang, N., Liu, R., Jiang, Y., Cheng, Y., and Li, B. (2019), "Shear-flow coupling characteristics of a three-dimensional discrete fracture network-fault model considering stress-induced aperture variations", *J. Hydrol.*, **571**, 416-424. https://doi.org/10.1016/j.jhydrol.2019.01.068.

Kulatilake, P.H.S.W. (1985), "Estimating elastic constants and strength of discontinuous rock", *J. Geotech. Eng.*, **111**(7), 847-864. https://doi.org/10.1061/(ASCE)0733-9410(1985)111:7(847).

Krauland, N., Soder, P. and Agmalm, G. (1989), "Determination of rock mass strength by rock mass classification-some experience and questions from boliden mines", *Int. J. Rock Mech. Min. Sci.*, **26**(1), 115-123. https://doi.org/10.1016/0148-9062(89)90531-7.

Khani, A., Baghbanan, A. and Hashemolhosseini, H. (2013), "Numerical investigation of the effect of fracture intensity on deformability and REV of fractured rock masses", *Int. J. Rock Mech. Min. Sci.*, **63**, 104-112. https://doi.org/10.1016/j.ijrmms.2013.08.006.

Long, J.C.S., Remer, J.S., Wilson, C.R. and Witherspoon, P.A. (1982), "Porous media equivalents for networks of discontinuous fractures", *Water Resour. Res.*, **18**(3), 645-658. https://doi.org/10.1029/wr018i003p00645.

Li, G. and Tang, C.A. (2015), "A statistical meso-damage mechanical method for modeling trans-scale progressive failure process of rock", *Int. J. Rock Mech. Min. Sci.*, **74**, 133-150. https://doi.org/10.1016/j.ijrmms.2014.12.006.

Lei, Q., Latham, J.P., Xiang, J. and Tsang, C.F. (2017), "Role of natural fractures in damage evolution around tunnel excavation in fractured rocks", *Eng. Geol.*, **231**, 100-113. https://doi.org/10.1016/j.enggeo.2017.10.013.

Laghaei, M., Baghbanan, A., Hashemolhosseini, H. and

Dehghanipoodeh, M. (2018), "Numerical determination of deformability and strength of 3D fractured rock mass", *Int. J. Rock Mech. Min. Sci.*, **110**, 246-256. https://doi.org/10.1016/j.ijrmms.2018.07.015.

Li, Y.C., Sun, S.Y. and Tang, C.A. (2019), "Analytical prediction of the shear behaviour of rock joints with quantified waviness and unevenness through wavelet analysis", *Rock Mech. Rock Eng.*, 1-13. https://doi.org/10.1007/s00603-019-01817-5.

Neuman, S.P. (1987), "Stochastic continuum representation of fractured rock permeability as an alternative to the RVE and fracture network concepts", *Proceedings of the 28th US Symposium of Rock Mechanics*, Tucson, U.S.A., July.

Oda, M. (1988), "A method for evaluating the representative elementary volume based on joint survey of rock masses", *Can. Geotech. J.*, **25**(3), 440-447. https://doi.org/10.1139/t88-049.

Oh, J., Moon, T., Canbulat, I. and Moon, J.S. (2019), "Design of initial support required for excavation of underground cavern and shaft from numerical analysis", *Geomech. Eng.*, **17**(6), 573-581. https://doi.org/10.12989/gae.2019.17.6.573.

Pouya, A. and Ghoreychi, M. (1998), "Determination of rock mass strength properties by homogenization", *Int. J. Numer. Anal. Meth. Geomech.*, **25**(13), 1285-1303. https://doi.org/10.1007/978-3-7091-2512-0-68.

Prudencio, M. and Jan, M.V.S. (2007), "Strength and failure modes of rock mass models with non-persistent joints", *Int. J. Rock Mech. Min. Sci.*, **44**(6), 890-902. https://doi.org/10.1016/j.ijrmms.2007.01.005.

Pariseau W.G., Puri, S. and Schmelter, S.C. (2008), "A new model for effects of impersistent joint sets on rock slope stability", *Int. J. Rock Mech. Min. Sci.*, **45**(2), 122-131. https://doi.org/10.1016/j.ijrmms.2007.05.001.

Ribacchi, R. (2000), "Mechanical tests on pervasively jointed rock material: Insight into rock mass behavior", *Rock Mech. Rock Eng.*, **33**(4), 243-266. https://doi.org/10.1007/s006030070.

Sarfarazi, V.H.H. and Alireza, B.S. (2017), "The effect of compression load and rock bridge geometry on the shear mechanism of weak plane", *Geomech. Eng.*, **13**(3), 431-446. https://doi.org/10.12989/gae.2017.13.3.431.

Shemirani, A.B., Haeri, H., Sarfarazi, V. and Hedayat, A. (2017), "A review paper about experimental investigations on failure behaviour of non-persistent joint", *Geomech. Eng.*, **13**(4), 535-570. https://doi.org/10.12989/gae.2017.13.4.535.

Tang, C.A. (1997), "Numerical simulation of progressive rock failure and associated seismicity", *Int. J. Rock Mech. Min. Sci.*, **34**(2), 249-261. https://doi.org/10.1016/S0148-9062(96)00039-3.

Vazaios, I., Farahmand, K., Vlachopoulos, N. and Diederichs, M. S. (2018), "Effects of confinement on rock mass modulus: A synthetic rock mass modelling (SRM) study", *J. Rock Mech. Geotech. Eng.*, **10**(3), 436-456. https://doi.org/10.1016/j.jrmge.2018.01.002.

Wang, M., Kulatilake, P.H.S.W., Um, J. and Narvaiz, J. (2002), "Estimation of REV size and three-dimensional hydraulic conductivity tensor for a fractured rock mass through a single well packer test and discrete fracture fluid flow modeling", *Int. J. Rock Mech. Min. Sci.*, **39**(7), 887-904. https://doi.org/10.1016/S1365-1609(02)00067-9.

Wong, R.H.C., Tang, C.A., Chau, K.T. and Lin, P. (2002), "Splitting failure in brittle rocks containing pre-existing flaws under uniaxial compression", *Eng. Fract. Mech.*, **69**(17), 1853-1871. https://doi.org/10.1016/S0013-7944(02)00065-6.

Wang, X.G., Jia, Z.X., Zhang, F.M. and Li, X.Q. (2010), *The Principle of Network Simulation of Rock Mass Structure and Its Engineering Application*, China Water Conservancy and Hydropower Press, Beijing, China.

Wang, P.T., Yang, T.H., Xu, T., Cai, M.F. and Li, C.H. (2016), "Numerical analysis on scale effect of elasticity, strength and failure patterns of jointed rock masses", *Geosci. J.*, **20**(4), 539-549. https://doi.org/10.1007/s12303-015-0070-x.

Wu, Z., Fan, L., Liu, Q. and Ma, G. (2017), "Micro-mechanical modeling of the macro-mechanical response and fracture behavior of rock using the numerical manifold method", *Eng. Geol.*, **225**, 49-60. https://doi.org/10.1016/j.enggeo.2016.08.018.

Wu, N., Liang, Z.Z., Li, Y.C., Li, H., Li, W.R. and Zhang, M.L. (2019), "Stress-dependent anisotropy index of strength and deformability of jointed rock mass: Insights from a numerical study", *Bull. Eng. Geol. Environ.*, 1-13. https://doi.org/10.1007/s10064-019-01483-5.

Xu, T., Ranjith, P.G., Wasantha, P.L.P., Zhao, J., Tang, C.A. and Zhu, W.C. (2013), "Influence of the geometry of partially-spanning joints on mechanical properties of rock in uniaxial compression", *Eng. Geol.*, **167**, 134-147. https://doi.org/10.1016/j.enggeo.2013.10.011.

Yang, S.Q. and Jing, H.W. (2011), "Strength failure and crack coalescence behavior of brittle sandstone samples containing a single fissure under uniaxial compression", *Int. J. Fract.*, **168**(2), 227-250. https://doi.org/10.1007/s10704-010-9576-4.

Yang, J.P., Chen, W.Z., Yang, D.S. and Yuan, J.Q. (2015a), "Numerical determination of strength and deformability of fractured rock mass by FEM modeling", *Comput. Geotech.*, **64**, 20-31. https://doi.org/10.1016/j.compgeo.2014.10.011.

Yang, X.X., Kulatilake, P.H.S.W., Jing, H.W. and Yang, S.Q. (2015b), "Numerical simulation of a jointed rock block mechanical behavior adjacent to an underground excavation and comparison with physical model test results", *Tunn. Undergr. Sp. Technol.*, **50**, 129-142. https://doi.org/10.1016/j.tust.2015.07.006.

Yu, Q.L., Zhu, W.C., Tang, C.A. and Yang, T.H. (2014), "Impact of rock microstructures on failure processes-Numerical study based on DIP technique", *Geomech. Eng.*, **7**(4), 375-401. https://doi.org/10.12989/gae.2014.7.4.375.

Zhang, W., Chen, J.P., Chen, H.E., Xu, D.Z. and Li, Y. (2013), "Determination of RVE with consideration of the spatial effect", *Int. J. Rock Mech. Min. Sci.*, **61**(7), 154-160. https://doi.org/10.1016/j.ijrmms.2013.02.013.

Zhou, J.R., Wei, J., Yang, T.H., Zhu, W.C., Li, L.C. and Zhang, P.H. (2018), "Damage analysis of rock mass coupling joints, water and microseismicity", *Tunn. Undergr. Sp. Technol.*, **71**, 366-381. https://doi.org/10.1016/j.tust.2017.09.006.

CC

Nomenclature

REV	Representative elementary volume of jointed rock masses
θ	The angle of the joint with the direction of the horizontal direction
U	Displacement loading
σ_p	Confining stress
σ_p/σ_c	Normalized confining stresses
K_i	Variation coefficient with model size i
A_i	Mechanical parameter with model size i

$\bar{A}_i$	Average mechanical parameter with model size greater than or equal to i
i	Model size
α	Joint dip angle
l	Joint trace length
(x_c, y_c)	Central coordinate of each trace line